

# Transient photoluminescence enhancement as a probe of the structure of impurity-trapped excitons in $\text{CaF}_2\text{:Yb}^{2+}$

Michael F. Reid,<sup>1</sup> Pubudu Senanayake,<sup>2</sup> Jon-Paul R. Wells,<sup>2,\*</sup> Giel Berden,<sup>3</sup>  
Andries Meijerink,<sup>4</sup> Alex Salkeld,<sup>2</sup> Chang-Kui Duan,<sup>5</sup> and Roger J. Reeves<sup>1</sup>

<sup>1</sup>*Department of Physics and Astronomy and MacDiarmid  
Institute for Advanced Materials and Nanotechnology,  
University of Canterbury, PB 4800, Christchurch 8140, New Zealand*

<sup>2</sup>*Department of Physics and Astronomy, University of Canterbury,  
PB 4800, Christchurch 8140, New Zealand*

<sup>3</sup>*FELIX Free Electron Laser Facility,  
FOM Institute for Plasmaphysics Rijnhuizen,  
PO Box 1207, 3430 BE, Nieuwegein, The Netherlands.*

<sup>4</sup>*Debye Institute for NanoMaterials Science, University of Utrecht,  
P.O. Box 80000, TA 3508 Utrecht, The Netherlands*

<sup>5</sup>*Department of Physics, University of Science  
and Technology of China, Hefei 230026, China*

(Dated: January 16, 2020)

## Abstract

We demonstrate a direct measurement of the energy levels of impurity-trapped excitons in  $\text{CaF}_2\text{:Yb}^{2+}$ . The radically different radiative decay rates of the lowest exciton state and higher excited states enable the generation of a transient photoluminescence enhancement measured via a two-step excitation process. We observe sharp transitions arising from changes of state of localized electrons, broad bands associated with changes of state of delocalized electrons, and broad bands arising from trap liberation.

PACS numbers: 76.30.Kg, 71.35.-y, 78.47.D-, 71.70.Ch

The unique optical properties of rare-earth doped materials are responsible for their crucial role in a wide variety of applications such as fluorescent tubes, white light LEDs, lasers, fiber amplifiers, and medical imaging [1, 2]. The sharp-line optical transitions within the  $4f^N$  ( $N = 0-14$ ) ground configurations of rare-earth ions have been extensively studied and may be accurately modelled [1–3]. Transitions involving excited configurations such as  $4f^{N-1}5d$  are crucial to many applications but information about these states is limited because  $4f^N \leftrightarrow 4f^{N-1}5d$  spectra consist of broad vibronic bands, yielding much less information than  $4f^N \leftrightarrow 4f^N$  spectra [4, 5]. Modern ab-initio methods [6, 7] are capable of accurately calculating excited-state electronic structure and bond-length variations, giving good agreement with available broad-band  $4f^N \leftrightarrow 4f^{N-1}5d$  spectra. The ab-initio calculations [7] indicate that transitions *between* the excited states would give a combination of sharp-line and broad vibronic transitions. We have recently proposed that two-color excitation experiments would give more detailed information about the excited states and better tests of the calculations [8].

Excited configurations of rare-earth ions are not restricted to  $4f^{N-1}5d$ . Configurations involving charge transfer between the rare-earth ion and other ions in the material are also important. Theoretical [6] and experimental [9] studies suggest that trapped excitons (where the excited electron becomes delocalized) play a crucial role in non-radiative processes.

In some  $\text{Eu}^{2+}$  and  $\text{Yb}^{2+}$  materials emission from excitonic states may be observed [10]. Excitonic emission in  $\text{CaF}_2$  and  $\text{SrF}_2$  doped with  $\text{Yb}^{2+}$  has been the subject of several studies [11–13]. The ground-state electronic configuration of  $\text{CaF}_2:\text{Yb}^{2+}$  is  $4f^{14}$ . UV excitation can promote one of the  $4f$  electrons to a  $5d$  orbital, giving the excited configuration  $4f^{13}5d$ . The  $5d$  electron rapidly becomes delocalized onto the next-nearest-neighbor  $\text{Ca}^{2+}$  ions. The  $\text{Yb}^{2+}$  is then effectively ionized to  $\text{Yb}^{3+}$ , with electronic configuration  $4f^{13}$ , i.e. one  $4f$  *hole*. This trivalent ion attracts the  $\text{F}^-$  nearest neighbors more strongly than a divalent ion, leading to a large contraction of bond length. Emission from the exciton states to the  $4f^{14}$  ground state involves the reverse change in bond length, and therefore a broad, structureless, red-shifted vibrational emission band [10]. Recent ab-initio calculations have given valuable insight into the quantum physics of exciton formation [6]. However, the broad bands yield no detailed information and experimental information on the energy-level structure of impurity-trapped excitons is largely deduced from indirect measurements such as temperature dependencies [11], pressure dependencies [9], and photoconductivity [13].

In this work we report on an investigation of the internal structure of impurity-trapped excitons using two-color measurements of single-crystal  $\text{CaF}_2$  doped with  $\text{Yb}^{2+}$ . By irradiating the crystal with IR radiation after exciting it with UV radiation we induce transitions between exciton states. Since some of the exciton excited states have much higher radiative rates than the lowest exciton state we can detect the excited state absorption by monitoring photoluminescence enhancement.

$\text{CaF}_2:\text{Yb}^{2+}$  crystals were grown using the vertical Bridgmann technique. Two-color measurements were made using UV output of a Quantronix TOPAS travelling-wave optical parametric amplifier (OPA) providing 3 ps pulses tunable in the 250-400 nm region of interest in this work at a repetition rate of 1 kHz. Pulsed infrared excitation was achieved using the Dutch FEL (FELIX) in Nieuwegein. The optical output of FELIX consists of a 4-6  $\mu\text{s}$  macropulse at a repetition rate of 10 Hz, containing micropulses at 25 MHz. FELIX is continuously tunable from 3 to 250  $\mu\text{m}$ . The OPA was synchronised to the FEL and the electronic timing between the two lasers could be varied. The UV and IR beams were spatially (but not temporally) overlapped on the sample, held at cryogenic temperatures within an Oxford instruments *microstat* helium flow cryostat. Subsequent UV/visible fluorescence was then detected using a TRIAX 320 spectrometer equipped with a C31034 photomultiplier.

Our results for 365 nm pulsed UV excitation of  $\text{CaF}_2:\text{Yb}^{2+}$  are consistent with previous work [11, 12], which reported strongly red-shifted fluorescence having a single-exponential decay with a lifetime of 15 ms at 4.2 K that reduces at higher temperatures.

In Fig. 1(a), the fluorescence spectra for  $\text{CaF}_2:\text{Yb}^{2+}$  at 10 K and 40 K are shown. At 10 K the band center and width (FWHM) are 17720, 3460  $\text{cm}^{-1}$ . At 40 K the intensity increases by a factor of 2.5 and the band center and width are 18380, 3240  $\text{cm}^{-1}$ . Previous analysis of the temperature dependence [11] suggests that the emission is from two states separated by about 40  $\text{cm}^{-1}$ , with very different radiative lifetimes, 15 ms for the lower state and 260  $\mu\text{s}$  for the upper state.

Emission bandwidths have been previously used to calculate the change in bond length between the lowest exciton state and the ground state as 0.17 Å [11]. The calculation is approximate because it uses an effective phonon frequency. A frequency of 325  $\text{cm}^{-1}$  gives a bond-length change of -0.17 Å for the lowest exciton state relative to the ground state (from our 10 K data) and -0.16 Å for the first excited exciton state (from our 40 K data). The first excited state thus has a *longer* bond length, closer to the ground state  $4f^{14}$  bond

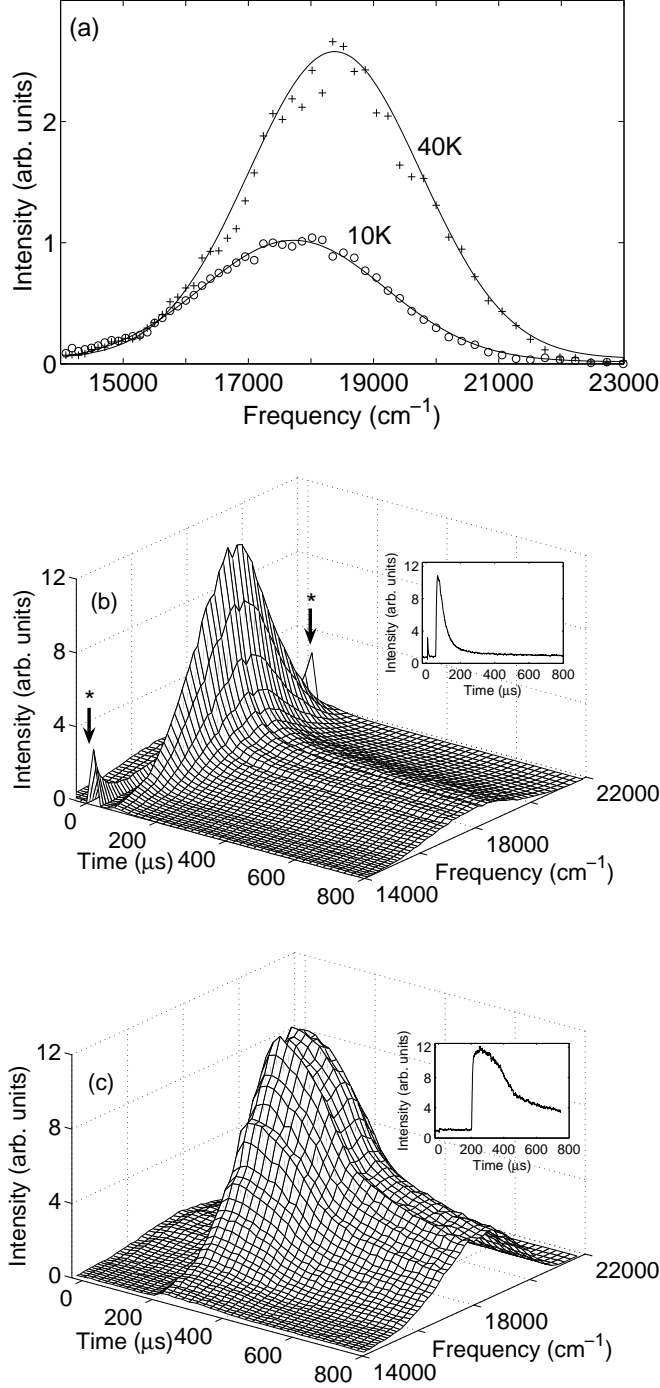


FIG. 1. Fluorescence from  $\text{CaF}_2:\text{Yb}^{2+}$  for excitation at 365 nm. (a) Spectra at 10 K and 40 K 900  $\mu\text{s}$  after UV excitation. (b) Time evolution of 10 K emission spectrum excited with 12.1  $\mu\text{m}$  ( $826 \text{ cm}^{-1}$ ) IR radiation following the UV pre-pulse. \* Shows a combination of first- and second-order UV scatter and emission from minor  $\text{Eu}^{2+}$  impurities. (c) Time evolution of 10 K emission spectrum excited with 16  $\mu\text{m}$  ( $625 \text{ cm}^{-1}$ ) IR radiation following the UV prepulse. The (b) and (c) insets show the time profile at peak emission wavelength.

length.

We now present the results of our two-color transient measurements at 10 K. Figs. 1(b) and 1(c) show respectively the results of irradiating the system at a wavelength of  $12.1\ \mu\text{m}$  ( $826\ \text{cm}^{-1}$ ) and  $16\ \mu\text{m}$  ( $625\ \text{cm}^{-1}$ ), delayed from the UV excitation by 100–200  $\mu\text{s}$ . The application of the IR pulse yields significant *enhancement* of the emission. Note that the IR pulse on its own cannot induce this optical emission. The enhancement occurs because we now populate excited excitonic states that have significantly *higher* radiative rates. An enhancement of the total emission at long time-scales is also observed, which we interpret as liberation of electrons from traps (discussed below), which is known to occur with intense IR radiation [14].

For  $12.1\ \mu\text{m}$  IR excitation there is a rise time of approximately 6  $\mu\text{s}$ , and a decay time of 43  $\mu\text{s}$ . The spectrum at the time corresponding to the maximum emission intensity is similar to the 40 K spectrum in Fig. 1(a). The enhanced emission is therefore likely to be a result of radiation from the state  $40\ \text{cm}^{-1}$  above the lowest exciton state. Further evidence for this conclusion is that at 40 K the IR excitation gives only a small enhancement and no change to the spectrum. The decay of the transient signal is much faster than the estimated 260  $\mu\text{s}$  radiative lifetime [11], due to non-radiative processes [12].

The spectral and temporal behaviour for  $16\ \mu\text{m}$  excitation, Fig. 1(c), is very different. The time development cannot be fitted by single exponential rise and decay times, but the rise time is approximately 30  $\mu\text{s}$  and the decay approximately 160  $\mu\text{s}$ . At the time corresponding to the maximum emission intensity we observe a mixture of low-energy and high-energy Gaussians. Several hundred  $\mu\text{s}$  after the IR excitation pulse the intensity of the low-energy Gaussian is still significantly more than before the IR pulse, suggesting that there are significantly *more* ions radiating than before the IR excitation.

The range of IR energies for which we have observed enhancement of the visible emission is shown in the excitation spectrum of Fig. 2(a), where the photoluminescence transient is time-integrated to give the signal. The spectrum consists of a broad band centered at  $650\ \text{cm}^{-1}$  and two sharper peaks at  $250\ \text{cm}^{-1}$  and  $1145\ \text{cm}^{-1}$ , with linewidths of 35 and 20  $\text{cm}^{-1}$  respectively. We note that dips in the broad band and the lower sharp peak correlate with atmospheric absorption of the FEL radiation which can distort the lineshape, despite purging of the IR beam path with dry  $\text{N}_2$  gas.

The temporal dynamics of the IR-induced signal being strongly dependent on the excita-

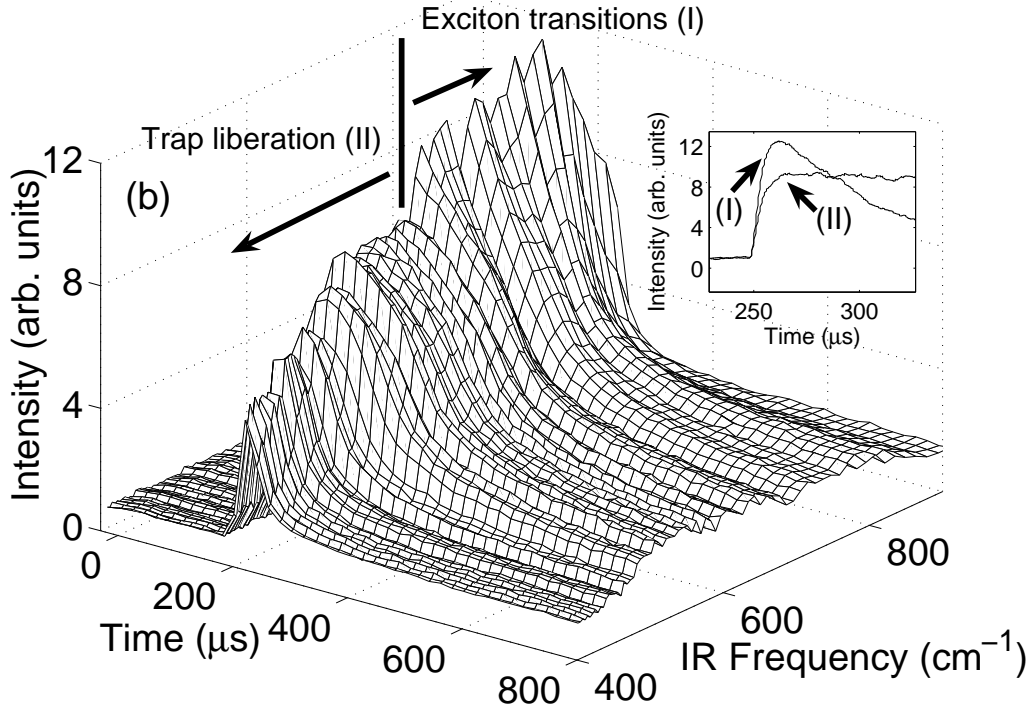
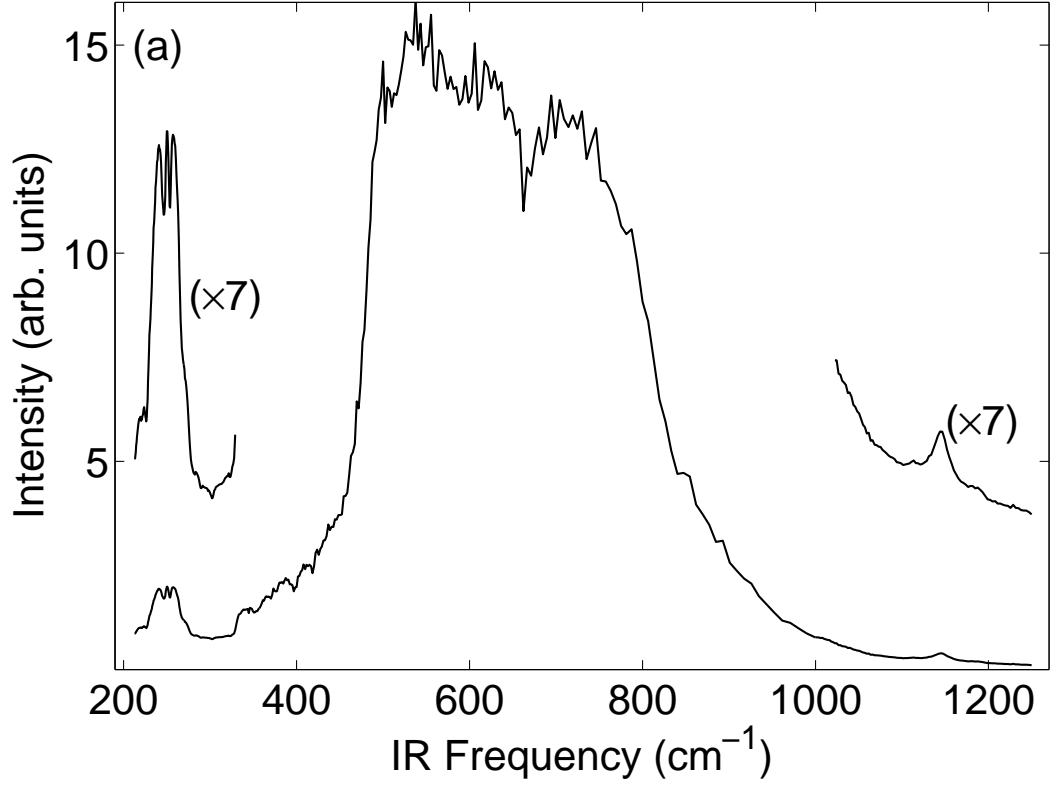


FIG. 2. (a) 10 K IR excitation spectrum of  $\text{CaF}_2:\text{Yb}^{2+}$  deduced by integrating emission enhancement over time. (b) Time-evolution of the 10 K IR excitation spectrum. Inset, rise time with (I) IR excitation at 825  $\text{cm}^{-1}$ , (II) IR excitation at 625  $\text{cm}^{-1}$

tion wavelength is further illustrated in figure 2(b). The broad peak is actually two distinct regions, a higher-energy region with fast rise and decay times, and a lower-energy region with slow rise and decay times. The long rise times may be attributed to trap liberation processes. A phenomenological model of a Coulomb trap having a threshold of  $380 \text{ cm}^{-1}$  gives an asymmetric spectrum with a width of approximately  $400 \text{ cm}^{-1}$  ([14] Eqn. (3)), which is consistent with the width of the low-energy band.

The high-energy part of the band, from  $650$  to  $950 \text{ cm}^{-1}$ , and the sharp lines, are assigned to transitions within the exciton. Recall that our exciton model is a  $\text{Yb}^{3+}$  ion with one  $4f$  hole ( $4f^{13}$ ) and a delocalized electron. It is the delocalized electron that can affect bonding, so the vibronic broadening of the  $650\text{--}950 \text{ cm}^{-1}$  band leads us to attribute this feature to transitions that change the orbital of the delocalized electron and therefore the bond length. The width of this band is similar to the width of the phonon spectrum in  $\text{CaF}_2$  [15], which implies that the bond-length change for the transition is small, similar to the difference in bond-length between the lowest two exciton states calculated above ( $0.01 \text{ \AA}$ ). An accurate calculation of the position and width of this band should be possible with a detailed ab-initio approach, as in Ref. [6].

The sharp excitation features observed at  $250$  and  $1145 \text{ cm}^{-1}$  cannot involve a change in bonding. We therefore assign them to changes in the wavefunction of the localized  $4f$  hole or the relative spin of the  $4f$  hole and delocalized electron. The latter is associated with an exchange Coulomb interaction. The calculations of Ref. [6] suggest that the excitons involve a linear combination of  $5d$  and  $6s$  orbitals with totally symmetric ( $s$ ) character. Unlike the  $\text{SrCl}_2:\text{Yb}^{3+}$  system [7] detailed calculations for  $\text{CaF}_2:\text{Yb}^{3+}$  are not available. However, we may model the sharp lines with a simple semi-empirical model by constructing a “crystal field” Hamiltonian for an  $s$  electron and a  $4f$  hole in a cubic crystal field,

$$H_{\text{cf}} = \zeta A_{\text{so}} + B^4 \left( C_0^4 + \sqrt{\frac{5}{14}} [C_4^4 + C_{-4}^4] \right) + B^6 \left( C_0^6 - \sqrt{\frac{7}{2}} [C_4^6 + C_{-4}^6] \right) + G^3(fs)g_3(fs), \quad (1)$$

where  $\zeta$  is the spin-orbit interaction for the  $4f$  electrons,  $B^4$  and  $B^6$  are crystal-field parameters for the  $4f$  electrons, and  $G^3(fs)$  the exchange interaction between the  $4f$  and the delocalized electron. Details of the Hamiltonian operators may be found in Refs. [3–5, 16]

Since we only observe two sharp lines it is not possible to fit all of the parameters in Eq.

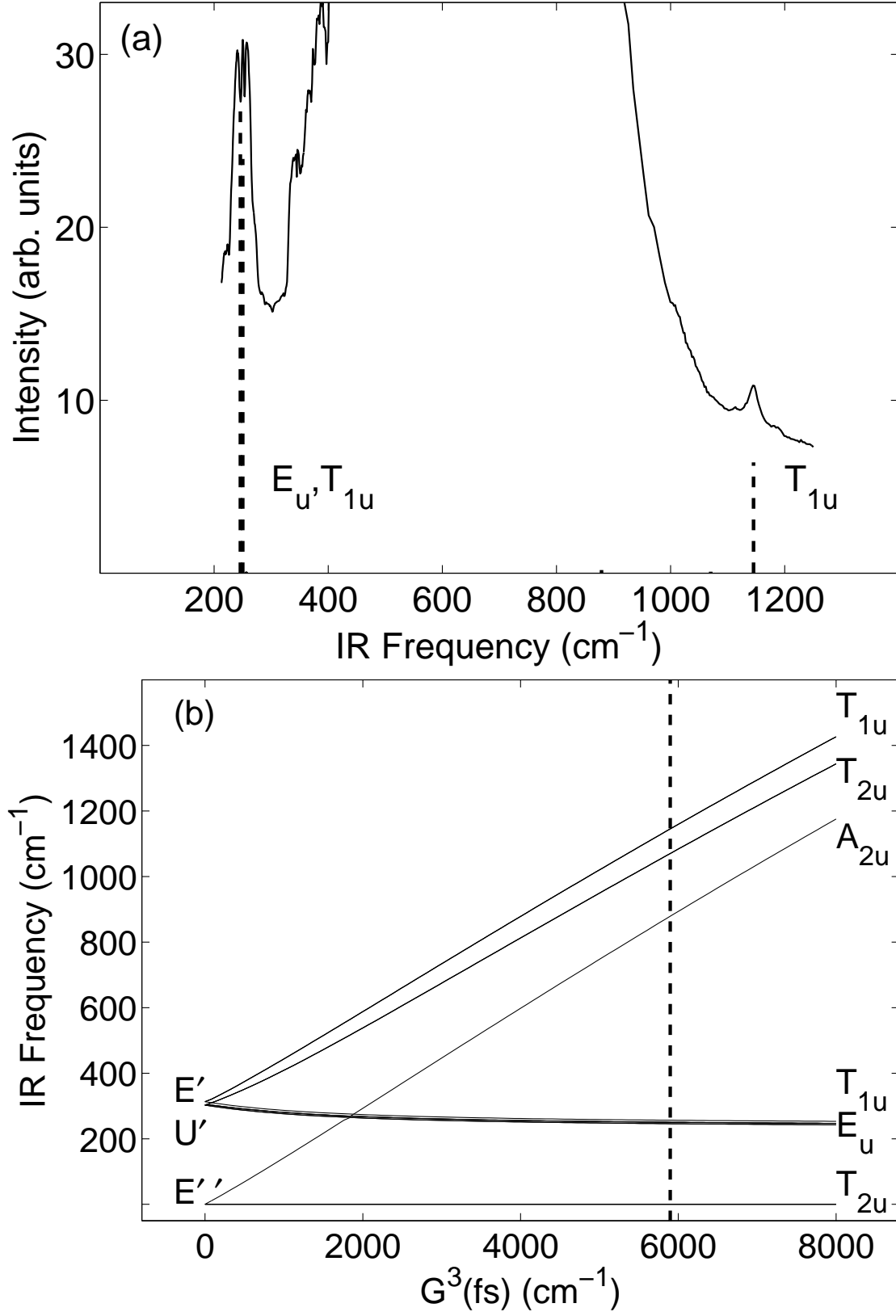


FIG. 3. (a) Calculated oscillator strengths for the transitions observed the IR excitation spectrum. (b) Dependence of the exciton energy levels on the exchange parameter  $G^3(\text{fs})$ .



(1). The spin-orbit parameter,  $\zeta$ , was fixed at  $2928 \text{ cm}^{-1}$ , the value determined for  $\text{Yb}^{3+}$  in  $\text{LaF}_3$  [3]. The ratio  $B^6/B^4$  was fixed at  $-0.35$ , the value obtained by Leśniak [17] for  $\text{Er}^{3+}$  in  $\text{CaF}_2$ . With these assumptions the parameter values  $B^4 = -800 \text{ cm}^{-1}$  and  $G^3(fs) = 5900 \text{ cm}^{-1}$  give energy levels that match the observed sharp lines.

Fig. 3 illustrates our calculation. When the  $G^3(fs)$  parameter is set to zero the  $^2F_{7/2}$  multiplet of  $4f^{13}$  splits into  $E''$ ,  $U'$  and  $E'$  irreducible representations of the octahedral group [18], as illustrated on the left side of Fig. 3(b). As  $G^3(fs)$  is increased these states couple with  $^2S$  (from the  $s$  electron). In cubic symmetry only magnetic dipole transitions are allowed. Calculated absorption oscillator strengths are compared with experiment in 3(a). Note that several transitions are forbidden or calculated to be very small.

The  $B^4$  parameter is similar to the value of  $-725 \text{ cm}^{-1}$  for the  $4f^{13}5d$  configuration of  $\text{Yb}^{2+}$  in  $\text{SrCl}_2$  [5]. A Hartree-Fock calculation using the atomic code of Cowan [16] gives  $G^3(fs) = 3167 \text{ cm}^{-1}$  for the  $4f^{13}6s$  configuration of  $\text{Yb}^{2+}$ . This is smaller than our experimental value. However, the calculations of Ref. [6] suggest that the exciton will contain mixtures of  $5d$  and  $6s$  orbitals. The exchange splitting for  $4f^{13}5d$  is over  $2000 \text{ cm}^{-1}$  [5], so our observed splitting of about  $1145 \text{ cm}^{-1}$  for the exciton, where the electron is in a more delocalized orbital than  $5d$ , is reasonable.

In conclusion, we have demonstrated that it is possible to probe the internal structure and dynamics of exciton states, and trap-liberation processes, in rare earth materials with a two-color selective fluorescence enhancement technique. A novel feature of our work is the observation of sharp-line transitions within the exciton. A quantitative account of these sharp line features has been obtained using a parametrized crystal-field model. Our observations provide a basis and motivation for detailed ab-initio calculations as in Ref. [6] and for investigation of other rare-earth excitonic systems using the same experimental approach.

This work was supported by the Marsden fund of the Royal Society of New Zealand via grant 09-UOC-080. We thank the Dutch FOM organisation for providing FELIX beamtime and thank the FELIX staff for their assistance. Mr P. Senanayake acknowledges the support of the University of Canterbury via a PhD studentship. C.-K. Duan is partially supported by the Natural Science Foundation of China, Grant No. 11074315.

---

\* Corresponding author: jon-paul.wells@canterbury.ac.nz

- [1] G. K. Liu and B. Jacquier, eds., *Properties of Rare Earths in Optical Materials* (Springer, 2005).
- [2] C. Ronda, ed., *Luminescence: From Theory to Applications* (Wiley-VCH, Weinheim, 2007).
- [3] W. T. Carnall, G. L. Goodman, K. Rajnak, and R. S. Rana, J. Chem. Phys., **90**, 3443 (1989).
- [4] G. W. Burdick and M. F. Reid, in *Handbook on the Physics and Chemistry of the Rare Earths*, Vol. 37, edited by K. A. Gschneidner Jr., J. C. Bunzli, and V. K. Percharsky (North Holland, 2007) Chap. 232, pp. 61–91.
- [5] Z. Pan, C. K. Duan, and P. A. Tanner, Phys. Rev. B, **77**, 085114 (2008).
- [6] G. Sánchez-Sanz, L. Seijo, and Z. Barandiarán, J. Chem. Phys., **133**, 114509 (2010).
- [7] G. Sánchez-Sanz, L. Seijo, and Z. Barandiarán, J. Chem. Phys., **133**, 114506 (2010).
- [8] M. F. Reid, L. Hu, S. Frank, C. K. Duan, S. Xia, and M. Yin, Eur. J. Inorg. Chem, **2010**, 26492654 (2010).
- [9] M. Grinbeg and S. Mahlik, J. Non-Cryst. Sol., **354**, 4163 (2008).
- [10] P. Dorenbos, J. Phys. Condensed Matter, **15** (2003).
- [11] B. Moine, B. Courtois, and C. Pedrini, J. Phys. France, **50**, 2105 (1989).
- [12] B. Moine, B. Courtois, and C. Pedrini, J.Lumin., **125**, 230 (1991).
- [13] C. Pedrini, M. F. Joubert, and D. S. McClure, J. Luminescence, **125**, 230 (2007).
- [14] I. Izeddin, M. A. J. Klik, N. Q. Vinh, M. S. Bresler, and T. Gregorkiewicz, Phys. Rev. Lett., **99**, 077401 (2007).
- [15] W. Hayes, M. C. K. Wiltshire, W. J. Manthey, and D. S. McClure, J. Phys. C, **6**, L273 (1973).
- [16] R. D. Cowan, *The Theory of Atomic Structure and Spectra* (U. California, Berkeley, 1981).
- [17] K. Leśniak, J. Phys.: Condens. Matter, **2**, 5563 (1990).
- [18] B. Henderson and G. F. Imbusch, *Optical spectroscopy of inorganic solids* (Clarendon Press, Oxford, 1989).